Controlled morphing of architected liquid crystal elastomer elements: modeling and simulations

Mechanics Research Communications. Year	Publication Office: Elsevier UK
Editor-in-Chief: A. Rosato New Jersey Institute of Technology, Newark, New Jersey, USA Anthony.Rosato@njit.edu	

Controlled morphing of architected liquid crystal elastomer elements: modeling and simulations

Mattia P. COSMA[1], Roberto BRIGHENTI[1*]

[1] *Department of Engineering and Architecture, University of Parma, Parco Area delle Scienze 181/A, 43124 Parma, Italy*

*corresponding author, e-mail: brigh@unipr.it
Tel.:+39-0521-905910; fax: +39-0521-905924

Abstract

Liquid crystal elastomers (LCE) are elastomeric materials possessing a network microstructure made of chains with a preferential orientation, induced by mesogen units embedded in the material prior to polymerization. This peculiarity can be harnessed to induce deformation of an LCE element by making its network switch from the preferentially oriented nematic state to the isotropic one, as occurs for instance by rising the temperature above a transition value characteristic of the material. This mechanism can be combined with an architected arrangement of LCE elements, whose nematic orientation and transition temperature are properly differentiated among the different zones constituting the element. In this way, interesting morphing capabilities can be obtained out of an architected elastomer made of LCE portions (ALCE), leading to a morphing structure whose deformation can be activated and precisely tuned by heating up or cooling down the material. In this research, we propose some simple architected LCE elements showing the capability of producing a variety of deformed shapes. A micromechanical theoretical model for LCE is firstly illustrated and several examples of morphing of architected LCE elements, whose mechanical response is obtained through finite element (FE) numerical analyses based on the proposed micromechanical model, are illustrated and critically discussed.

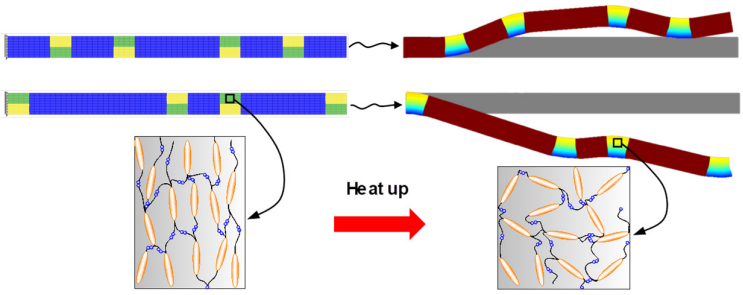

Keywords: liquid crystal elastomers, stimuli-responsive materials, architected materials, morphing.

1. Introduction

To date, the possibility to produce materials showing particular intriguing properties, such as the controllable responsiveness to external stimuli or actions, has stimulated a huge research efforts, especially in the field of small-scale technological applications [1], [2]. In this context, the capability of stimuli responsive materials of exhibiting large deformations leading to a noticeable shape change when properly stimulated (the so-called morphing), offers the potentiality to fabricate smart devices (nowadays also enabled by the available 3D printing technologies [3]), providing new attractive functionalities. These shape-change capabilities

have been exploited, for instance, in soft robots where complex motions and shape-change (exploited to obtain bending, twisting and extension) are provided by the structure itself, leading to a system with an unlimited number of degree of freedoms, without the need of an external tethered control as typically occurs for standard robots [4].

Several examples of controlled structural shape morphing, i.e. of structures that change shape in a controlled manner, can be found in the literature; for instance, some modular self-reconfigurable robots can morph from a snake-like structure into a quadruped walker or vice versa, thus allowing the robot to move through a narrow space to accomplish its tasks [5]. In nature, the complex motion of soft muscular structures can be achieved by a synergic actuation of many simple contractile elements, properly spatially and functionally arranged [6]. The morphing capability has also been obtained by harnessing the tensegrity concept through a modular design, coupling elastomeric cables, made of memory polymers, with strut elements, [7]. Morphing has also been obtained by exploiting differential surface wetting in soft structures or by assembling materials with different fluid diffusion length scales [8]. Residual stresses induced by some polymerization processes, such as the photopolymerization one, have shown the capability to provide structures with shape morphing characteristics, enabled by the shrinkage and distortion of the fabricated samples induced by a non-uniform laser exposure during the production process [9]. Finally, it is worth mentioning that morphing capabilities have also been obtained within the field of origami and kirigami functional materials [10],[11].

Among the materials and structures enabling shape morphing, liquid crystal elastomers (LCEs) represent a charming class of responsive polymers that combine mechanical properties of both fluids and solids [12]-[19]. In this context, experimental researches have shown the possibility to obtain shape programmable actuators through direct-write printed 3D structures with a controlled molecular order [20]-[22].

They exhibit large and reversible deformations when properly stimulated by environmental inputs; if we zoom into their microstructure, in some conditions a spontaneous order given by the molecular structure of liquid crystals (LCs) can be observed (nematic state), while in other conditions they exhibit a disordered configuration of the chain network, typical of standard polymeric matrices (isotropic state). Being the ordered-disordered transition phenomenon (nematic to isotropic) accompanied by large and reversibile deformations of the network, this class of material has been recognized to be particularly attractive for actuation and morphing [23]. As a matter of fact, in LCEs the ordered-disordered transition is usually triggered by heat or light (Fig. 1), leading to – when LCE elements are properly arranged – a responsive morphing material or device suitable for actuation.

The so-called nematic order is usually quantified through the order tensor, describing the alignment of the mesogen units at the microscopic scale [16].

Depending on the type of LCE in turn, the variation of the nematic order can be induced by different triggering stimuli,

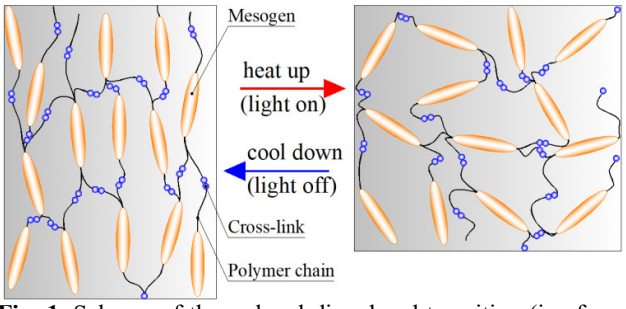

Fig. 1. Scheme of the ordered-disordered transition (i.e. from the nematic to the isotropic state) in a LCE element.

ranging from heat, UV-light, electric or magnetic field [24]-[26].

For instance, the irradiation of the material with UV-light (photo-actuation mechanism), modifies the chemical structure of the LC when it contains molecular units undergoing isomerization (such as the trans-cis isomerization taking place in azobenzene-based LCEs), while the nematic-isotropic switching can be obtained by directly heating the material in which temperature-sensible mesogens have been embedded [27]. Phase transition can be also obtained by light irradiation of LCEs doped with photo-thermal agents (such as gold nanoparticles, carbon nanotubes, graphene etc.), leading to the photo-thermal actuation [28]-[31].

By harnessing the deformation capabilities of LCEs and by taking inspiration from the so-called metamaterials – whose properties come from the arrangement of their building blocks rather than of their mechanical properties, [32],[33]) – we investigate the quantitative tunability of a class of metamaterials, obtained by properly arranging LCE units, capable of showing a wide variety of controllable shape morphing induced by a temperature change. In the following, we refer to the above-mentioned elements as architected liquid crystal elastomers (ALCEs). By analogy with deformations occurring in nature for locomotion or peristaltic motion, we demonstrate the possibility to realize structural elements whose deformed shapes resemble that observed in several natural phenomena, and that can be precisely controlled by changing the relevant environmental stimulus.

For this purpose, we introduce a theoretical model that, through a statistical-based description of the network chains arrangement, leads to a micromechanical model suitable to describe the mechanical response of polymers with a varying nematic order pattern.

In the literature, various models have been proposed to predict the shape produced by changing the mesogens alignment in LCEs, allowing the inverse problem of designing the alignment patterns for prescribed morphing shapes to be solved. Theoretical models based on the relationship between the local orientation of the mesogen units in thin sheets or in simple bilayers and the arising curvature have been developed [34],[35].

A stretch–temperature relation has been implemented into a FE (finite element) approach to model the shape morphing of LCEs; this approach has been used in [37] where experimental tests related to the photothermal light-induced shape-morphing of LCEs with a proper spatial pattern of gold nanoparticles concentration has been simulated.

In the present approach, we follow a different route: the statistical distribution of the polymer chains driven by the mesogens arrangement (depending on the local temperature of the LCEs and, if it is the case, on the mechanical stress applied), is used to determine the local stress and the deformation state of the material. No structural models have been introduced (such as the assumption typically made for thin plates, membrane or bilayer structural elements) and so from this viewpoint the proposed approach is suitable to model any arrangement of LCEs patterns with different mesogen orientation and/or transition temperature.

The proposed micromechanical model is then upscaled at the continuum level and implemented within a FE framework for the simulation of real case elements.

Various arrangements of LCE blocks – characterized by different nematic orders and, eventually, by different transition temperatures – are considered, and their shape morphing capabilities are quantitatively simulated through numerical analyses. It is shown how, by properly tuning some properties of the material at the mesoscale level (such as the arrangement of the constituent block of ALCEs or more intriguingly, and as a novelty, their transition temperature), a controlled morphing of structural elements can be achieved. Although the inverse problem of designing a specific pattern of mesogens in order to obtain a prescribed shape-morphing is not a goal of the present work, the developed model is exploited for clearly and quantitatively illustrate, by adjusting the LCE pattern and transition temperature, how vast can be the obtainable responsiveness of a simple structural beam-like element.

From this perspective, this study provides an insight into the limitless possibilities to obtain the desired conformation out of properly designed architected LCEs.

The paper is organized as follows: Sect. 2 deals with the mechanics of stimulus-responsive LCEs while Sect. 3 illustrates the basic idea of architected liquid crystal elastomers. Some numerical simulations are presented in Sect. 4 and, finally, Sect. 5 outlines some conclusions and future perspectives.

2. Mechanical behavior of stimulus-responsive LCE

2.1. Statistical based description of a polymer network

Standard polymer network consists of an amorphous arrangement of entangled linear chains – each one assumed to be made of N rigid (Khun's) segments of equal length b, arranged in space according to the random-walk theory – whose physical state, according to the Freely-Join-Chain (FJC) assumption, depends only on the so called end-to-end vector $\boldsymbol{r}$ [16],[38]. The chains are linked together at discrete points, termed as cross-links, forming the network. The chain arrangement in the 3D space, quantified by the statistical distribution $\rho_0(\boldsymbol{r})$ of the end-to-end vectors $\boldsymbol{r}$, allows to determine the mechanical state of the polymer [38]. In the stress-free state, the distribution of the end-to-end vectors is usually assumed to follow the standard 3D Gaussian distribution, i.e. $\rho_0(\boldsymbol{r}) = c_a\,\varphi_0(\boldsymbol{r})$, being c_a the number of mechanically active chains (i.e. chains joined to the network at both of their extremities), and φ_0 the normalized Gaussian distribution function, $\varphi_0(|\boldsymbol{r}|) = \left(\frac{3}{2\pi N b^2}\right)^{\frac{3}{2}} \exp\left(-\frac{3|r|^2}{2Nb^2}\right)$, [23].

The knowledge of the distribution change, from the stress-free state to the actual one (accounting for the mechanical deformation of the network, and eventually for chains breakage, time-related effects as well as the ordered-disordered network transition occurring in LCEs), provides all the information required to describe the mechanical state of the polymer in the current state [39].

In polymer physics, the mechanical energy stored in a single chain is usually assumed to depend on the end-to-end vector length $|\boldsymbol{r}|$. According to the Gaussian statistics [40], valid for moderate chain stretch values, the elastic energy of a single chain is expressed as $\psi(\boldsymbol{r}) = \frac{3k_BT}{2Nb^2}|\boldsymbol{r}|^2$, so the potential elastic energy per unit volume of the polymer, evaluated with respect to the stress-free state, is given by:

$$\Delta\Psi = \Psi - \Psi_0 = \int_\Omega [\rho(\boldsymbol{r},t) - \rho_0(\boldsymbol{r})]\psi\, d\Omega \tag{1}$$

Alternatively, Eq. (1) can be rewritten as follows [16],[38],[39]:

$$\Delta\Psi = \frac{3c_a k_B T}{2Nb^2}\mathrm{tr}(\boldsymbol{\mu} - \boldsymbol{\mu}_0) + p[\det \boldsymbol{F} - 1] \tag{2}$$

where p is the hydrostatic pressure required to enforce the incompressibility constraint (expressed by $\det \boldsymbol{F} = 1$, being $\boldsymbol{F}$ the deformation gradient tensor) here assumed. In Eq. (2) the distribution tensors, having the meaning of the covariance matrices of the distribution of $\boldsymbol{r}$ in the current and in the initial stress-free state, $\boldsymbol{\mu} = \langle\varphi\, \boldsymbol{r}\otimes\boldsymbol{r}\rangle$, $\boldsymbol{\mu}_0 = \langle\varphi_0 \boldsymbol{r}\otimes\boldsymbol{r}\rangle$, have been introduced, while $\langle\blacksquare\rangle$ represents the integration of $\blacksquare$ over the chain configuration space [39]. If the affine deformation hypothesis holds true, the chain stretch vector is given by $\boldsymbol{\lambda} = \boldsymbol{r}/|\boldsymbol{r}_0|$ and the distribution tensor in the current state becomes $\boldsymbol{\mu} = \langle\varphi\, \boldsymbol{\lambda}\otimes\boldsymbol{\lambda}\rangle\, |\boldsymbol{r}_0|^2$. Such a tensor contains the information related to the average chain stretch in different directions; in its principal directions frame of reference identified by the versors $\boldsymbol{m}_i$, it is written as $\boldsymbol{\mu}_d = \mu_i\, \boldsymbol{m}_i \otimes \boldsymbol{m}_i$ ($i = 1,2,3$) where μ_i are the eigenvalues of $\boldsymbol{\mu}$ and the Einstein summation convention has been used. The distribution tensor $\boldsymbol{\mu}$ provides the information related to the spatial distribution of the network chains and so every action influencing such a distribution reflects on $\boldsymbol{\mu}$ whose knowledge suffices to know the mechanical state of the polymer.

2.2. Thermally-driven chains rearrangement: from standard polymer network to LCE

When a LCE polymer network in the nematic state is considered, its mesogens units are preferentially oriented in one direction, say along the $x-$direction of the Cartesian frame of reference, i.e. $m_1 \equiv x$, and the normalized Gaussian function of the polymer chain distribution φ_0 is non-isotropic; the so-called order parameter is defined as $Q = \langle\frac{3}{2}\cos^2\theta - \frac{1}{2}\rangle$

[16] (where θ is the angle formed by the mesogen axes and their average direction of alignment) and the distribution tensor becomes:

$$\boldsymbol{\mu}_d = \frac{Nb^2}{3}\begin{bmatrix} 1+2Q & 0 & 0 \\ 0 & 1-Q & 0 \\ 0 & 0 & 1-Q \end{bmatrix} \tag{3}$$

When the mesogen units are perfectly aligned along the $x-$axis then $Q = 1$ (θ is either equal to 0 or π), while the value $Q = 0$ indicates randomly oriented rods as occurs in a perfectly isotropic arrangement of chains for which $\langle \cos^2\theta \rangle = 1/3$ and $\boldsymbol{\mu} = \frac{Nb^2}{3}\,\mathbf{1}$. Values of Q falling in the range $0 \div 1$ indicate a not perfect alignment, whose degree of dispersion about the main direction increases as $Q \to 0$. Finally, when $Q = -1/2$, all the LC rods belong to the $y-z$ plane. If the director varies in space, it is convenient to introduce the tensor order parameter $Q_{ij} = \langle \frac{3}{2} u_i u_j - \frac{1}{2}\delta_{ij} \rangle$ where u_i is the unit vector representing the direction of the considered mesogen [16],[14].

Finally, the stress state of the material is provided by [42]:

$$\boldsymbol{\sigma} = J^{-1}\boldsymbol{P}\boldsymbol{F}^T = \frac{3c_a k_B T}{Nb^2}(\boldsymbol{\mu} - \boldsymbol{\mu}_0) + p\,\mathbf{1}, \quad \boldsymbol{P} = \frac{\partial \Delta\Psi}{\partial \boldsymbol{F}} \tag{4}$$

where $\boldsymbol{\sigma}$, $\boldsymbol{P}$ are the Cauchy and the first Piola stress tensors, respectively, and $J = \det \boldsymbol{F}$. It is worth mentioning that, when a LCE network is considered, the distribution tensor which appears in the definition of the stress state of the material (Eq. (4)), must be assessed accordingly. In this case, the initial distribution tensor of the nematic LCE network, assumed herein to coincide with the stress-free state of the material, is $\boldsymbol{\mu}_0 = \boldsymbol{\mu}(t=0) = \boldsymbol{\mu}_d(Q = Q_0)$, see Eq. (3). The current distribution tensor $\boldsymbol{\mu}(t)$ is affected by both the order change induced by the temperature variation as well as by the applied mechanical deformation; thus, its time rate $\dot{\boldsymbol{\mu}}(t)$ can be expressed by adding up these two above-mentioned contributions:

$$\dot{\boldsymbol{\mu}}(t) = \dot{\boldsymbol{\mu}}_m(t) + \dot{\boldsymbol{\mu}}_T(t) \tag{5}$$

where $\dot{\boldsymbol{\mu}}_m$ represents the effect of the mechanical stress while $\dot{\boldsymbol{\mu}}_T$ is the rate associated with the temperature-dependent change of the nematic order. The above rates are given by [41]:

$$\dot{\boldsymbol{\mu}}_m = \frac{\partial \boldsymbol{\mu}(t)}{\partial t}\Big|_T = \langle \varphi(t)\, \boldsymbol{r} \otimes \boldsymbol{r} \rangle\, \boldsymbol{L}(t)\, \boldsymbol{\mu}(t) + [\boldsymbol{L}(t)\, \boldsymbol{\mu}(t)]^T \tag{6a}$$

$$\dot{\boldsymbol{\mu}}_T(t) = \frac{\partial \boldsymbol{\mu}(t)}{\partial t}\Big|_m = 2\frac{Nb^2}{3}\left[\dot{\boldsymbol{Q}}(t) - \boldsymbol{W}(t)\boldsymbol{Q}(t) + \boldsymbol{Q}(t)\,\boldsymbol{W}(t)\right] \tag{6b}$$

where $\blacksquare|_T$, $\blacksquare|_m$ indicate the quantity $\blacksquare$ evaluated at constant temperature and at zero mechanical stress, respectively, while $\boldsymbol{W} = \frac{1}{2}(\nabla \dot{\boldsymbol{u}} - \nabla \dot{\boldsymbol{u}}^T)$ is the spin tensor. The distribution tensor $\boldsymbol{\mu}$ at the generic time t can be obtained by integrating the above rates in $(0, t)$ as $\boldsymbol{\mu}(t) = \boldsymbol{\mu}(0) + \int_0^t \left[\dot{\boldsymbol{\mu}}_m(\tau) + \dot{\boldsymbol{\mu}}_T(\tau)\right] d\tau$.

In the case the order parameter depends on the temperature while the principal directions of $\boldsymbol{Q}$ do not change, $\dot{\boldsymbol{Q}}(t)$ in Eq. (6b) is given by

$$\dot{\boldsymbol{Q}}(t) = \frac{1}{2}\frac{\dot{\boldsymbol{\ell}}(t)}{b} \tag{7}$$

with $\dot{\boldsymbol{\ell}}(t) = b\dot{Q}(t)\,[3\,\boldsymbol{n} \otimes \boldsymbol{n} - \mathbf{1}]$, $\dot{Q}(t) = \frac{\partial Q(T)}{\partial T}\dot{T}$

being $\boldsymbol{n}$ the nematic director and $\boldsymbol{\ell}$ is the so called step length tensor.

The nematic order of the LCE can be related to the temperature of the material in such a way that $Q = Q_0$ when $T < T_{NI}$, while $Q \to 0$ if $T > T_{NI}$, where T and T_{NI} are the current and the nematic-isotropic transition temperature, respectively, while Q_0 is the initial value of the order parameter of the LCE network.

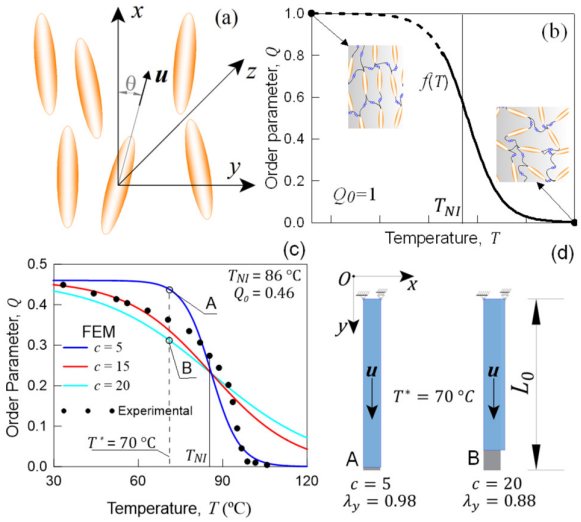

Fig. 2. (a) Scheme of the preferential orientation of liquid crystal molecules fluctuating around the director $n_1 \equiv x$. (b) Ordered-disordered transition in LCE due to a temperature increase (from left to right). (c) $Q-T$ curves obtained through the function $f(T)$ for different values of the material-dependent parameter c, compared with experimental values [43]. (d) Deformed shapes of the considered element at a given T for two values of the parameter c (obtained from FEM results) .

The $Q-T$ relationship, to be used for determining the nematic-isotropic evolution counterpart of the distribution tensor (see Eq. (6b), depends on the physical-chemical properties of the material and can be determined from experimental tests [44]; it quantifies the transition of the order parameter from its initial value Q_0 to the current one at the temperature T. Here, we adopt an expression for $Q-T$ in the form $Q(T) = Q_0\, f(T)$, with $f(T) = \left[1 + \exp\frac{T - T_{NI}}{c}\right]^{-1}$, being c a material-dependent parameter.

The $Q-T$ curves provided by the model obtained by assuming different values of the parameter c, are shown in Fig. 2(c); the comparison with the experimentally obtained order parameter measured on a monodomain nematic elastomer ($y-$oriented) shows a reasonable similar trend. Starting from a known nematic configuration with $Q_0 = 0.46$ at $T = 20\,°C$, we heat up the material up to a temperature above the nematic-transition temperature $T_{NI} = 86\,°C$ [43] in order to recover the isotropic state. The material-dependent parameter c influences the nematic-isotropic transition, leading to sharp transitions (lower values

of c) or more gradual ones (higher values of c), Fig. 2(c). The deformed shapes of the strip resulting from FEM analysis, for two values of c at a given temperature $T^* = 70$ °, are reported in Fig. 2(d): the contraction along the nematic direction is lower for lower c ($\lambda_y = 0.98$, A) since Q remains practically unchanged until this temperature value is reached ($c = 5$, point A, Fig. 2(c)); on the other hand, at the same temperature, Q is lower for a higher c (point B, Fig. 2(c)) corresponding to a more evident contraction ($\lambda_y = 0.88$, B, Fig. 2(d)).

3. From bio-inspired morphing to architected liquid crystal elastomers

3.1. Bio-inspired materials architectures

The fascinating architectures of natural structures (ranging from wood, antler, bone and teeth, silk, fish scales, bird beaks, insect wings, shells, etc.) are increasingly attracting the interest of researchers because of their mechanical functionality and effectiveness. In fact, the above-mentioned structures have usually an optimum weight to strength ratio, allowing to safely bear mechanical stress by using the least amount of material. On the other hand, soft-bodied animals (such as octopus, caterpillars, snakes, maggots, etc.) are able to deform in a complex way to get a desired functionality; among the most useful capabilities in nature, locomotion represents a crucial task to be efficiently done for survival purpose. Morphing strategy represents an efficient way for small organism to move in a viscous fluid where the kinematic-reversible mechanism, typically used at high Reynolds numbers, doesn't work. Soft natural living matter is thus a source of inspiration for the development of engineered artificial materials and devices mimicking functionalities observable in nature [45]-[48].

Natural structures display intricate architectures – ranging from the nano-, micro- and meso-scale size – reflecting an impressive range of different functionalities; the arrangement, orientations and features of individual structural units is often optimized to get the best overall behavior, consisting in the maximization of survival and longevity, by performing in the best way basic biological functions or by protecting themselves by the surrounding [49]. Natural structures properly respond to certain environmental conditions or to peculiar external stimuli: examples are represented by "pill bugs" (armadillidium vulgare, terrestrial isopods), capable of morphing for protecting themselves against predators by means of conglobation morphing, the ability to roll up into a ball when stimulated by strong vibrations or pressure exerted by predators.

It is worth mentioning that morphing in nature can also take place in a more general way; social animals (such as fire ants, honey bees, etc.) can aggregate in swarms by joining many individuals [50], so forming a super-organism (or cluster) whose shape can change according to different stimuli in order to fulfill some goal such as mechanical stability or thermal comfort [51],[52]. Opposite to the above-cited collective behavior, single cell organisms (such as individual cells) morph to produce motility [53]. Inspired by morphing of highly deformable organisms, the development of continuum materials whose architecture is made of blocks with a controllable deformation, paves the way to create simple and efficient soft actuators with unlimited morphing capabilities.

3.2. LCE-based metamaterials

When properly stimulated, the deformation potentialities of LCEs offer the opportunity to create architected elements by a suitable assembling of LCE portions having different nematic order orientation and/or transition temperatures; this allows for the production of soft actuators whose morphing capability can be precisely tuned [27],[54]. The production of such architected LCE-based elements, is nowadays possible and affordable thanks to the modern additive manufacturing production technologies [21],[22],[24],[55],[56]. The easiest way to get a shape morphing LCE-based metamaterial is obtainable by arranging LCE elements characterized by distinct nematic order orientations, into a bilayer structure, showing a bending-like deformation through the thickness expansion/contraction mismatch. This allows to get, but is not limited to, wavy-like deformed shapes. A first experimental attempt to mimic the wavy-like morphing of an element can be found in [57], where two LCE layers joined together have been used to induce bending morphing.

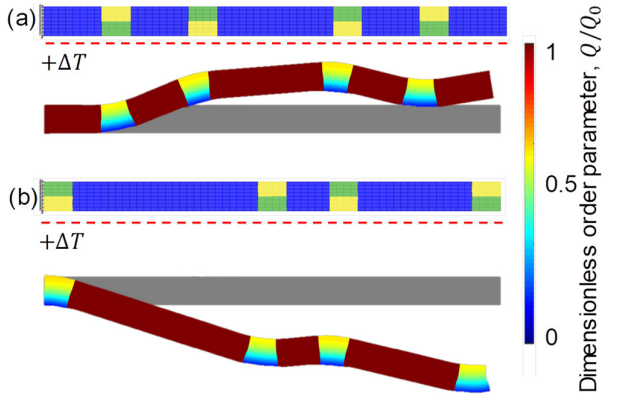

Fig. 3. Examples of generic deformed shapes, provided by the present model, obtainable by temperature-triggered morphing of an element made of properly arranged LCE parts with different nematic order orientations.

In other words, the deformations in adjacent parts of LCE form hinges providing a localized rotation induced by alternate tensile/compressive strain along the thickness; such a controllable rotations, coupled with inert parts of material (blue blocks of Fig. 3), affect the shape of the whole element, allowing to get different overall conformations according to the LCE arrangement within the element itself (Fig. 3).
Being LCE-based actuators capable of developing an actuation power of the order of 10^5 J/m^3 [58], they offer the possibility of being employed in a variety of applications, such as in soft robots, tunable stereoscopic displays, intelligent skin, grippers, etc.

4. Numerical simulations

4.1. Numerical implementation

The micromechanical model illustrated above can be readily implemented into a FE computational framework. The variational statement of the problem reads:

$$\delta_{\boldsymbol{u}}\Pi = \delta_{\boldsymbol{u}}\Psi_e + \delta_{\boldsymbol{u}}\Psi_{ext} = \int_{\mathcal{B}_0} \frac{\partial \Psi}{\partial \nabla \boldsymbol{u}} \delta \nabla \boldsymbol{u}\, dV - \int_{\mathcal{B}_0} \boldsymbol{B}\cdot\delta\boldsymbol{u}\, dV - \int_{\partial\mathcal{B}_0} \boldsymbol{t}\cdot\delta\boldsymbol{u}\, dA = \int_{\mathcal{B}_0} [\nabla\cdot\boldsymbol{P} - \boldsymbol{B}]\delta\boldsymbol{u} dV + \int_{\partial\mathcal{B}_0} [\boldsymbol{P}\cdot\boldsymbol{N} - \boldsymbol{t}]\cdot\delta\boldsymbol{u} dA = 0 \quad (8)$$

being $\boldsymbol{P} = \boldsymbol{J\sigma F^{-T}} = \boldsymbol{\partial\Psi/\partial\nabla u}$ the first Piola stress tensor, while $\boldsymbol{B}, \boldsymbol{t}$ are the body and traction forces in the reference configuration and $\boldsymbol{N}$ is the unit outward normal to the boundary. By introducing the FE discretization of the displacement field and of its gradient,

$$\boldsymbol{u}_a = \sum_{i=1}^{n_n}[N]_i\,\tilde{\boldsymbol{u}}_i,\quad \nabla\cdot\boldsymbol{u}_p = \nabla_X \sum_{i=1}^{n_n}[N]_i\tilde{\boldsymbol{u}}_i = \sum_{i=1}^{n_n}[B]_i\tilde{\boldsymbol{u}}_i \quad (9)$$

(being $\blacksquare_a$ and $\tilde{\blacksquare}$ the interpolated and the nodal values of the quantity $\blacksquare$) the above variational statement (8) leads to the following equilibrium equation written in terms of the unbalanced or nodal residual force vector

$$\{R\}^e_{\boldsymbol{u}} = \int_{V_0^e}[B]^T\boldsymbol{P}\, dV - \int_{V_0^e}[N]^T\boldsymbol{B}dV + \int_{A_0^e}[N]^T\boldsymbol{t}dA = \{0\} \quad (10)$$

where the single finite element e with volume V_0^e and boundary surface A_0^e has been considered. It can be noticed that the knowledge of the stress field at the FE Gauss points allows evaluating the vector of the unbalanced residual forces whose norm has to be made to fulfill some convergence requirements through a iterative procedure for example by using the standard Newton method [41].

4.2. Numerical simulations and discussion

This section is devoted to illustrate some ALCE morphing results obtained by performing numerical simulations; the examined cases, consisting in a simple structural rectangular 2D strip element made of LCEs units – alternatively arranged by changing their director direction – outline the huge variety of morphing shapes obtainable from architected liquid crystal elastomers. The use of a simple structural element, allows capturing and highlighting the various controlled morphing outcome obtainable by different arrangement of nematic mesogens patterns, and of their transition temperature. Elements made of LCE blocks arranged as shown in Fig. 4 are considered, each one characterized by distinct widths of the constituent LCE blocks, namely $w/L = 0.125; 0.25; 0.5$ (Fig. 4). The height of each LCE block is assumed to be one half of the height of the strip and is kept fixed for the three patterns investigated. As can be appreciated from the zoom detail of Fig. 4, the strip is assumed to be obtained by assembling blocks of LCE having different nematic orientations, namely LC_Y blocks (green regions in Fig. 4) and the LC_X (yellow regions in Fig. 4), corresponding to mesogen units aligned along the y-axis and x-axis, respectively. We investigate the role played by different relative sizes of LCE rectangular units within the ALCE element, whose nematic mesogens orientations and/or nematic-isotropic transition temperatures T_{NI} are different from block to block, in producing different morphing shapes for different boundary constraints.

We consider first a strip made of a pattern of appropriately assembled LCEs blocks having the same T_{NI}. Then, we illustrate the morphing capability of an element made of a fixed pattern of LCEs blocks but having different T_{NI}.

In all the examples, we consider a rectangular strip made of LCE blocks whose geometry in the undeformed state is characterized by $L/h = 16$, $h = 500\ \mu m$ and thickness $t = h$. Moreover, we adopt a constant shear modulus of the material $\mu = 13.33\ kPa$ that, for sake of simplicity, is assumed to be independent of temperature. The analyses are performed by assuming a plane stress condition for the material and a fast heating because of the small size of the element. In the examples, the temperature of the bottom surface of the strip is increased from $T_B = 25\ °C$ to $T_B = 150\ °$. The temperature evolution within the material is determined by solving the heat conduction problem in the element's domain whose thermal conductivity and specific heat are assumed to be $\kappa = 0.2$ W/mK and $C = 1050$ J/Kg K, respectively. The thermal expansion of the material is neglected within the temperature range considered, in order to not have further deformations not related to the phase change of the LCE parts.

Unless differently stated, we assume the nematic-isotropic transition temperature to occur at $T_{NI} = 50\ °C$, while the parameters describing the transition from the initial nematic to the final isotropic state are assumed to be $Q_0 = 0.3$ and $c = 20$ for all the LCEs blocks.

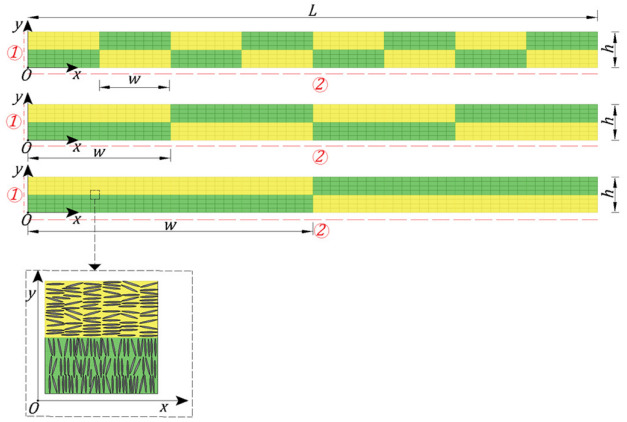

Fig. 4. Arrangement of LCE blocks with two nematic order orientations, yellow along x, green along y, organized in architected patterns; three different dimensionless ratios w/L are adopted.

We implemented the micromechanical model outlined above into a FE framework for simulating the morphing behavior [26]; firstly, we investigate the morphing response of ALCE strips, assumed to be fabricated according to the three patterns shown in Fig. 4. The deformation response is studied by adopting either a clamped boundary condition (BC) along the edge ① (displacements $\delta_x = \delta_y = 0$ at $X = 0$) or a simply supported element along the edge ②, i.e. lying on a

rigid horizontal frictionless plane (unilateral constraint, displacements $\delta_y \geq 0$ at $Y = 0$), see Fig. 4.

The results related to the cantilever elements are reported in Fig. 5; the deformed shapes of the centreline for three different temperature levels ($T_B/T_{NI} = 0.7; 1.0; 1.5$) and the corresponding deformed shapes of the element for $T_B/T_{NI} = 1$ for the three patterns of Fig. 4 ($w/L = 0.125, 0.25, 0.5$), are illustrated. As can be noticed, coupling of LCE blocks in a proper architected way provides alternate zone of compressive/tensile strain within the element, resulting in a wavy morphing of the element. Further, it can be appreciated that the right-hand side of the strip move upwards during the temperature rising: at a fixed T_B/T_{NI} value, the higher the w/L, the higher the uplift displacement obtained.

We consider now the results related to the architected LCE strips lying on a rigid frictionless plane; Fig. 6 shows the LCE-temperature-dependent deformation, leading to a morphing of the elements governed by wavy-like deformed shapes whose amplitudes depend on the ratio w/L.

In this case, due to the different BCs compared to those of the cantilever element strips, the amplitude of the deformed shapes are less pronounced at a fixed values of w/L and T_B/T_{NI}.

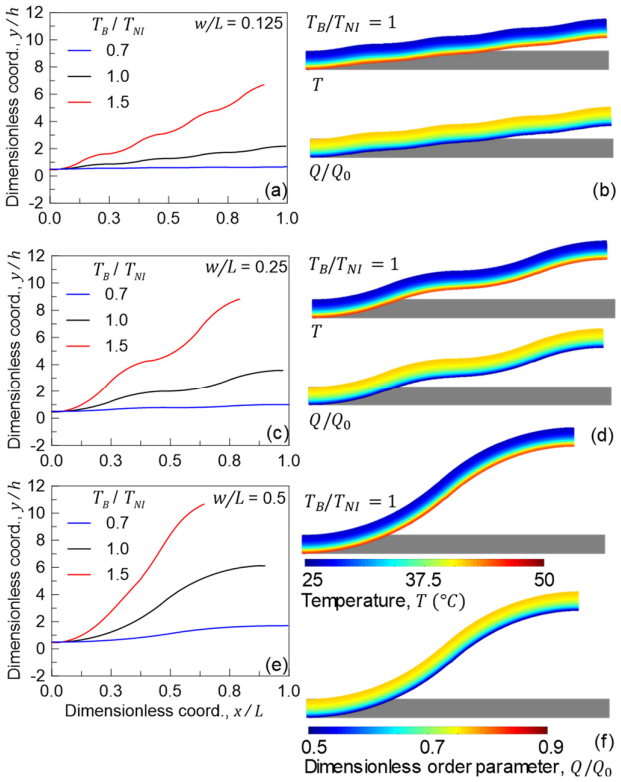

Fig. 5. Architected LCE cantilever strip element under a temperature increase (see Fig. 4). (a,c,e) centerline deformed shapes, and corresponding deformed shapes with temperature and nematic order fields at $T_B/T_{NI} = 1$ (b,d,f).

In the last example, we consider the morphing of a cantilever strip whose LCE elements have both different nematic orientation and transition temperatures; $T_{NI,X} = 50°C$ has been assumed for zones with mesogens preferentially oriented along X, while $T_{NI,Y}$ is equal to either $50, 70, 100, 130°C$ for zones with mesogens preferentially oriented along Y (cases no. 1, 2, 3, 4, respectively, in Fig. 7a,b). This leads to a controlled morphing of the element, allowing, for example, to make the point P_0 of the element (see Fig. 7a) capable of following a desired path. Let's image to require the point P_0 to move from its initial position ($X = L, Y = 0$) to an assumed target zone (see the light-blue circle in Fig. 7a). The use of LCE blocks with different activation temperatures $T_{NI,Y}$ allows the point P to move from P_0 to the target area moving upward to the left (black paths, $T_{NI,Y} = 50, 70°C$) or first downward and then upward to the left (red paths, $T_{NI,Y} = 100,130°C$), making the point, for instance, capable of moving toward the desired region by avoiding the eventual presence of obstacles.

5. Conclusions and future developments

We have quantitatively investigated the possibility to precisely control the shape morphing of elements made of architected blocks of LCE (ALCEs), showing the possibility to obtain several functionalities. It has been considered a temperature-responsive LCE whose transition from the nematic state to the isotropic one occurs when the transition temperature is overcome.

A general theoretical micromechanical-based framework, without any particular assumptions coming from the structural element in turn, has been briefly illustrated and some numerical FE simulations, based on

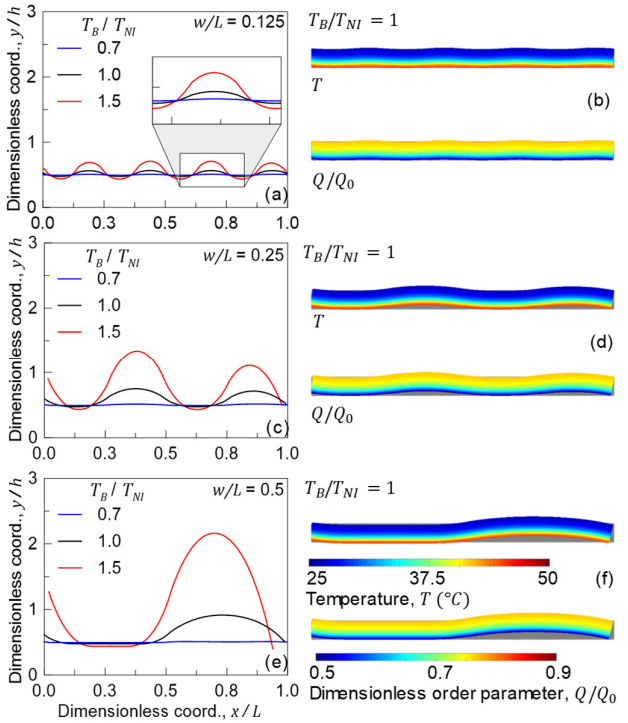

Fig. 6. Architected LCE strip lying on a horizontal frictionless plane (see Fig. 4) activated by a temperature increase. (a,c,e) centerline deformed shapes, and corresponding deformed shapes with temperature and nematic order fields at $T_B/T_{NI} = 1$ (b,d,f).

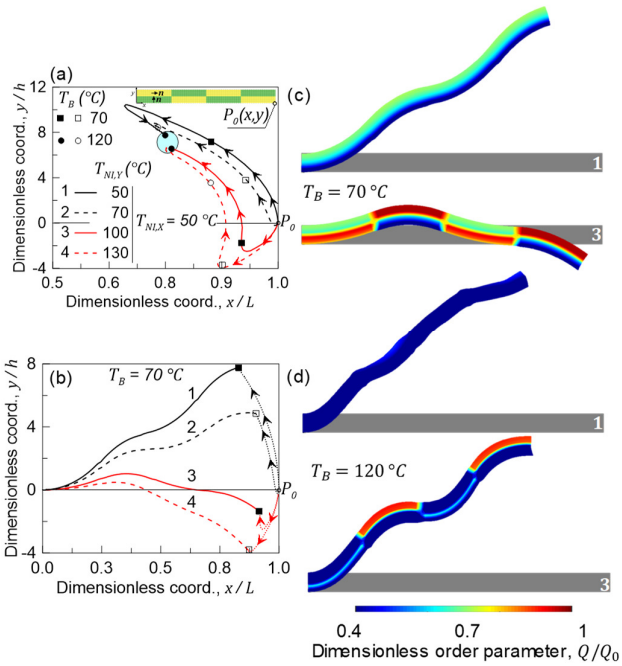

Fig. 7. Architected LCE cantilever strip activated by a temperature increase. (a) paths of the point P obtained by rising the temperature T_B from 20°C to 120°C, (b) centerline deformed patterns and (c,d) corresponding element's deformed shapes with dimensionless nematic order maps.

the FE implementation of the proposed theory, have been performed. It has been demonstrated that a proper arrangement of the LCE blocks with different nematic order orientations and/or transition temperatures, allows us to induce quite different deformed shapes, leading to a desired morphing and making the deformation process capable to follow a preferential path. The present investigation, which considers a simple structural element, allows us to predict quantitatively the role played by the nematic orientations and transition temperatures pattern and represents a promising way to obtain fully tunable flexible systems displaying large reversible deformations with path-controllable displacements. The obtained results represent a starting point for the design and simulation of more complex engineering systems and devices. A future important advancement will be the design of the proper LCE pattern arrangement, capable of producing a desired deformed shape under a given temperature history. This complex issue (suitable to be tackled by using, for example, Artificial Intelligence algorithms) is a so-called inverse problem, consisting in finding the architecture of a LCE-based metamaterial (whose design space consists of LCE blocks geometry and their spatial arrangement, mesogens orientation and activation temperature) according to the desired morphing functionality.

References

[1] D. Roy, J.N. Cambre, B.S. Sumerlin, Future perspectives and recent advances in stimuli-responsive materials, Progress in Polymer Science. 35 (2010) 278–301. https://doi.org/10.1016/j.progpolymsci.2009.10.008.

[2] R. Brighenti, Y. Li, F.J. Vernerey, Smart polymers for advanced applications: a mechanical perspective review, Frontiers in Materials. 7 (2020) 196. https://doi.org/10.3389/fmats.2020.00196.

[3] R. Brighenti, M.P. Cosma, L. Marsavina, A. Spagnoli, M. Terzano, Laser-based additively manufactured polymers: a review on processes and mechanical models, Journal of Materials Science. (2020). https://doi.org/10.1007/s10853-020-05254-6.

[4] S. Mintchev, D. Floreano, Adaptive Morphology: A Design Principle for Multimodal and Multifunctional Robots, IEEE Robotics Automation Magazine. 23 (2016) 42–54. https://doi.org/10.1109/MRA.2016.2580593.

[5] R. Pfeifer, M. Lungarella, F. Iida, Self-organization, embodiment, and biologically inspired robotics., Science. 318 (2007) 1088–1093. https://doi.org/10.1126/science.1145803.

[6] E.T. Roche, R. Wohlfarth, J.T.B. Overvelde, N.V. Vasilyev, F.A. Pigula, D.J. Mooney, K. Bertoldi, C.J. Walsh, A bioinspired soft actuated material, Advanced Materials. 26 (2014) 1200–1206. https://doi.org/10.1002/adma.201304018.

[7] M. Chen, J. Liu, R.E. Skelton, Design and control of tensegrity morphing airfoils, Mechanics Research Communications. 103 (2020) 103480. https://doi.org/10.1016/j.mechrescom.2020.103480.

[8] M. Pezzulla, S.A. Shillig, P. Nardinocchi, D.P. Holmes, Morphing of geometric composites via residual swelling, Soft Matter. 11 (2015) 5812–5820. https://doi.org/10.1039/C5SM00863H.

[9] A.A. Bauhofer, S. Krödel, J. Rys, O.R. Bilal, A. Constantinescu, C. Daraio, Harnessing photochemical shrinkage in direct laser writing for shape morphing of polymer sheets, Advanced Materials. 29 (2017) 1703024. https://doi.org/10.1002/adma.201703024.

[10] Y. Zhu, M. Birla, K.R. Oldham, E.T. Filipov, Elastically and Plastically Foldable Electrothermal Micro-Origami for Controllable and Rapid Shape Morphing, Advanced Functional Materials. 30 (2020) 2003741. https://doi.org/10.1002/adfm.202003741.

[11] L. Jin, A.E. Forte, B. Deng, A. Rafsanjani, K. Bertoldi, Kirigami-Inspired Inflatables with Programmable Shapes, Advanced Materials. 32 (2020) 2001863. https://doi.org/10.1002/adma.202001863.

[12] H. Sackmann, Franklin D. Saeva. Liquid Crystals - the Fourth State of Matter. Marcel Dekker, Inc., New York and Basel; 1979 491 Seiten. Preis SFr. 106.-, Kristall Und Technik. 16 (1981) 527–527. https://doi.org/10.1002/crat.19810160421.

[13] P.-G. de Gennes: Physique moléculaire - réflexions sur un type de polymères nématiques, Comptes rendus de l'Académie des Sciences B 281, 101-103 (1975)

[14] P.-G. De Gennes, J. Prost, The physics of liquid crystals, Oxford university press, 1993.

[15] P. Bladon, E.M. Terentjev, M. Warner, Transitions and instabilities in liquid crystal elastomers, Phys. Rev. E 47 (1993) R3838–40. https://doi.org/10.1103/PhysRevE.47.R3838.

[16] M. Warner, E.M. Terentjev, Liquid crystal elastomers, Oxford University Press, 2007.

[17] J. Kupfer, H. Finkelmann, Nematic liquid single crystal elastomers, Macromol Chem Rapid Commun 12 (1991) 717–726. https://doi.org/10.1002/marc.1991.030121211.

[18] A. De Simone, L. Teresi, Elastic energies for nematic elastomers, The European Physical Journal E 29 (2009) 191–204. https://doi.org/10.1140/epje/i2009-10467-9.

[19] Y. Zhang, C. Xuan, Y. Jiang, Y. Huo, Continuum mechanical modeling of liquid crystal elastomers as dissipative ordered solids, Journal of the Mechanics and Physics of Solids 126 (2019) 285–303. https://doi.org/10.1016/j.jmps.2019.02.018.

[20] T. White, D. Broer, Programmable and adaptive mechanics with liquid crystal polymer networks and elastomers, Nature Materials 14 (2015) 1087–1098. https://doi.org/10.1038/nmat4433.

[21] C.P. Ambulo, J.J. Burroughs, J.M. Boothby, H. Kim, M.R. Shankar, T.H. Ware, Four-dimensional printing of liquid crystal elastomers, ACS applied materials & interfaces. 9(42) (2017) 37332–37339. https://doi.org/10.1021/acsami.7b11851.

[22] M. Barnes, S.M. Sajadi, S. Parekh, M.M. Rahman, P.M. Ajayan, R. Verduzco, Reactive 3D printing of shape-programmable liquid crystal elastomer actuators, ACS Applied Materials & Interfaces. 12(25) (2020) 28692–28699. https://doi.org/10.1021/acsami.0c07331.

[23] M. Barnes, R. Verduzco, Direct shape programming of liquid crystal elastomers, Soft Matter. 15 (2019) 870–879. https://doi.org/10.1039/C8SM02174K.

[24] S.K. Ahn, T.H. Ware, K.M. Lee, V.P. Tondiglia, T.J. White, Photoinduced topographical feature development in blueprinted azobenzene-functionalized liquid crystalline elastomers, Advanced Functional Materials. 26(32) (2016) 5819–5826. https://doi.org/10.1002/adfm.201601090.

[25] T. Ikeda, M. Nakano, Y. Yu, O. Tsutsumi, A. Kanazawa, Anisotropic bending and unbending behavior of azobenzene liquid-crystalline gels by light exposure, Advanced Materials. 15(3) (2003) 201–205. https://doi.org/10.1002/adma.200390045.

[26] C. Huang, J. Lv, X. Tian, Y. Wang, Y. Yu, J. Liu, Miniaturized

Swimming Soft Robot with Complex Movement Actuated and Controlled by Remote Light Signals, Scientific Reports. 5 (2015) 17414. https://doi.org/10.1038/srep17414.

[27] A. Kotikian, C. McMahan, E.C. Davidson, J.M. Muhammad, R.D. Weeks, C. Daraio, J.A. Lewis, Untethered soft robotic matter with passive control of shape morphing and propulsion, Science Robotics. 4 (2019). https://doi.org/10.1126/scirobotics.aax7044.

[28] J. Xu, S. Chen, W. Yang, B. Qin, X. Wang, Y. Wang, ... & Y. Dong, Photo actuation of liquid crystalline elastomer nanocomposites incorporated with gold nanoparticles based on surface plasmon resonance, Soft matter. 15(30) (2019) 6116-6126. https://doi.org/10.1039/C9SM00984A.

[29] H. Kim, J.A. Lee, C.P. Ambulo, H.B. Lee, S.H. Kim, V.V. Naik, ... & T.H. Ware, Intelligently actuating liquid crystal elastomer carbon nanotube composites, Advanced Functional Materials. 29(48) (2019) 1905063. https://doi.org/10.1002/adfm.201905063.

[30] Y. Yang, W. Zhan, R. Peng, C. He, X. Pang, D. Shi, ... Z. Lin, Graphene-enabled superior and tunable photomechanical actuation in liquid crystalline elastomer nanocomposites, Advanced Materials. 27(41) (2015) 6376-6381. https://doi.org/10.1002/adma.201503680.

[31] H.K. Bisoyi, A.M. Urbas, Q. Li, Soft Materials Driven by Photothermal fect and Their Applications, Advanced Optical Materials. 6 (2018) 1800458. https://doi.org/10.1002/adom.201800458.

[32] Q. Zhang, D. Zhang, Y. Dobah, F. Scarpa, F. Fraternali, R.E. Skelton, Tensegrity cell mechanical metamaterial with metal rubber, Appl. Phys. Lett. 113 (2018) 031906. https://doi.org/10.1063/1.5040850.

[33] M. Kadic, G.W. Milton, M. van Hecke, M. Wegener, 3D metamaterials, Nature Reviews Physics. 1 (2019) 198–210. https://doi.org/10.1038/s42254-018-0018-y.

[34] C. Mostajeran, Curvature generation in nematic surfaces, Physical Review E. 91(6) (2015) 062405. https://doi.org/10.1103/PhysRevE.91.062405.

[35] F. Feng, J.S. Biggins, M. Warner, Evolving, complex topography from combining centers of Gaussian curvature, Physical Review E. 102(1) (2020) 013003. https://doi.org/10.1103/PhysRevE.102.013003.

[36] J.A. Lewis, R.G. Nuzzo, L. Mahadevan, A.S. Gladman, E.A. Matsumoto, Biomimetic 4D printing, Nat. Mater. 15 (2016) 413-418. https://doi.org/10.1038/nmat4544.

[37] A.S. Kuenstler, Y. Chen, P. Bui, H. Kim, A. DeSimone, L. Jin, R.C. Hayward, Blueprinting photothermal shape-morphing of liquid crystal elastomers, Advanced Materials. 32(17) (2020) 2000609. https://doi.org/10.1002/adma.202000609.

[38] M. Doi, Introduction to polymer physics, Oxford University Press, 1996.

[39] F.J. Vernerey, R. Long, R. Brighenti, A statistically-based continuum theory for polymers with transient networks, Journal of the Mechanics and Physics of Solids. 107 (2017) 1–20. https://doi.org/10.1016/j.jmps.2017.05.016.

[40] M. Rubinstein, R.H. Colby, Polymer Physics, Oxford University Press, 2003.

[41] R. Brighenti, C. G. McMahan, M. P. Cosma, A. Kotikian, J.A. Lewis, C. Daraio, A micromechanical-based model of stimulus responsive liquid crystal elastomers, J. Sol. & Struct.219 (2021), 92-105. https://doi.org/10.1016/j.ijsolstr.2021.02.023.

[42] R. Brighenti, M.P. Cosma, Swelling mechanism in smart polymers responsive to mechano-chemical stimuli, Journal of the Mechanics and Physics of Solids. 143 (2020) 104011. https://doi.org/10.1016/j.jmps.2020.104011.

[43] S.M. Clarke, A. Hotta, A.R. Tajbakhsh, E.M. Terentjev, Effect of crosslinker geometry on equilibrium thermal and mechanical properties of nematic elastomers., Phys Rev E Stat Nonlin Soft Matter Phys. 64 (2001) 061702. https://doi.org/10.1103/PhysRevE.64.061702.

[44] A.R. Tajbakhsh, E.M. Terentjev, Spontaneous thermal expansion of nematic elastomers, The European Physical Journal E. 6 (2001) 181–188. https://doi.org/10.1007/s101890170020.

[45] U.G.K. Wegst, H. Bai, E. Saiz, A.P. Tomsia, R.O. Ritchie, Bioinspired structural materials, Nature Materials. 14 (2015) 23–36. https://doi.org/10.1038/nmat4089.

[46] C. Laschi, M. Cianchetti, B. Mazzolai, L. Margheri, M. Follador, P. Dario, Soft Robot Arm Inspired by the Octopus, Null. 26 (2012) 709–727. https://doi.org/10.1163/156855312X626343.

[47] D. Rus, M.T. Tolley, Design, fabrication and control of soft robots, Nature. 521 (2015) 467–475. https://doi.org/10.1038/nature14543.

[48] M. Wehner, R.L. Truby, D.J. Fitzgerald, B. Mosadegh, G.M. Whitesides, J.A. Lewis, R.J. Wood, An integrated design and fabrication strategy for entirely soft, autonomous robots, Nature. 536 (2016) 451–455. https://doi.org/10.1038/nature19100.

[49] K. Oliver, A. Seddon, R.S. Trask, Morphing in nature and beyond: a review of natural and synthetic shape-changing materials and mechanisms, Journal of Materials Science. 51 (2016) 10663–10689. https://doi.org/10.1007/s10853-016-0295-8.

[50] F.J. Vernerey, E. Benet, L. Blue, A.K. Fajrial, S.L. Sridhar, J.S. Lum, G. Shakya, K.H. Song, A.N. Thomas, M.A. Borden, Biological active matter aggregates: Inspiration for smart colloidal materials, Advances in Colloid and Interface Science. 263 (2019) 38–51. https://doi.org/10.1016/j.cis.2018.11.006.

[51] O. Peleg, J.M. Peters, M.K. Salcedo, L. Mahadevan, Collective mechanical adaptation of honeybee swarms, Nature Physics. 14 (2018) 1193–1198. https://doi.org/10.1038/s41567-018-0262-1.

[52] R. Wagner, T. Shen, F. Vernerey, K. Such, E. Hobbs, Construction of non-equilibrium structures by insect aggregations: the case of fire ants, Bulletin of the American Physical Society. 65 (2020).

[53] V.S. Deshpande, R.M. McMeeking, A.G. Evans, A bio-chemo-mechanical model for cell contractility, Proceedings of the National Academy of Sciences. 103 (2006) 14015–14020. https://doi.org/10.1073/pnas.0605837103.

[54] M.J. Ford, C.P. Ambulo, T.A. Kent, E.J. Markvicka, C. Pan, J. Malen, T.H. Ware, C. Majidi, A multifunctional shape-morphing elastomer with liquid metal inclusions, Proceedings of the National Academy of Sciences. 116 (2019) 21438–21444. https://doi.org/10.1073/pnas.1911021116.

[55] A. Kotikian, R.L. Truby, J.W. Boley, T.J. White, J.A. Lewis, 3D Printing of Liquid Crystal Elastomeric Actuators with Spatially Programed Nematic Order, Advanced Materials. 30 (2018) 1706164. https://doi.org/10.1002/adma.201706164.

[56] Z. Wang, Z. Wang, Y. Zheng, Q. He, Y. Wang, S. Cai, Three-dimensional printing of functionally graded liquid crystal elastomer, Science advances. 6(39) (2020) eabc0034. https://doi.org/10.1126/sciadv.abc0034.

[57] M. Wang, X.-B. Hu, B. Zuo, S. Huang, X.-M. Chen, H. Yang, Liquid crystal elastomer actuator with serpentine locomotion, Chem. Commun. 56 (2020) 7597–7600. https://doi.org/10.1039/D0CC02823A.

[58] A.R. Tajbakhsh, E.M. Terentjev, Spontaneous thermal expansion of nematic elastomers, The European Physical Journal E. 6(2) (2001) 181-188. https://doi.org/10.1007/s101890170020.